Proceedings of the ASME 2013 32nd International Conference on Ocean, Offshore and Arctic Engineering
OMAE2013
June 9-14, 2013, Nantes, France

OMAE2013-11453

HEAT TRANSFER MODELING AND APPLICATION OF GAS-LIQUID TWO-PHASE FLOW IN PARTIALLY-BURIED PIPELINE

Kai Wang[*] *Qingping Li*

Research Institute of China National Offshore Oil Corporation
Beijing, P.R China

Abstract

For the deepwater partially-buried pipeline transporting wet natural gas, a mechanistic heat transfer model is developed, and the temperature profile behaviors and corrosion resistant alloy (CRA) length of deepwater pipelines of Liwan3-1 gas field are studied by numerical simulation. The result shows that for a critical temperature of 23 °C, all production flowlines should be used CRA, and the CRA length of the tieback pipeline is recommended to be 1.5 km. There are significant differences of temperature drop between the mechanistic and linear models.

1 Introduction

The Liwan3-1 gas field, which is in 1,500 meters water depth and approximately 300 km south of Hong Kong, is the first deepwater gas field in China. Following concept screening studies, the subsea production system has been chosen. That all subsea wells are tied back to a fixed platform on the continental shelf, approximately 80km north of the 3-1-1 well, will provide the most robust solution for development of the offshore facilities to achieve First Gas by end of 2012, and with the greatest flexibility for further development of other nearby prospects. The east & west production flowlines and subsea tieback pipelines (SSTB) are sketched in Fig. 1.

For the deepwater flowlines and pipelines transporting wet natural gas, one of the serious problems is that the CO_2 of fluid compositions is more than 3 moles%, moreover the corresponding partial pressure of CO_2 can be up to 600 kPa, which is a threat to flow assurance. Generally, compared to corrosion inhibitors, pH stabilizers, corrosion allowance and other means, corrosion resistant alloys (CRA) is good to guard against “condensate water corrosion” but has a high price, several times more than carbon steel. Therefore, the combination of “CRA + carbon steel” is chosen to the production flowlines and SSTB of Liwan3-1 gas field. Namely, only when the fluid temperature is higher than "critical temperature", below which no condensate water generated, the CRA pipe is chosen, and the carbon steel pipe for the other segments. The optimal CRA length should be to meet a balance between the anticorrosion reliability and cost. Thus, it is the key to predict the critical point along the pipeline accurately at which the fluid temperature is nearly equal to the critical temperature. Usually, a deepwater pipeline is in the partially-buried state after some years and is assumed to be fully exposed for calculation of temperature profile, under which a faster temperature drop and shorter CRA length are presented.

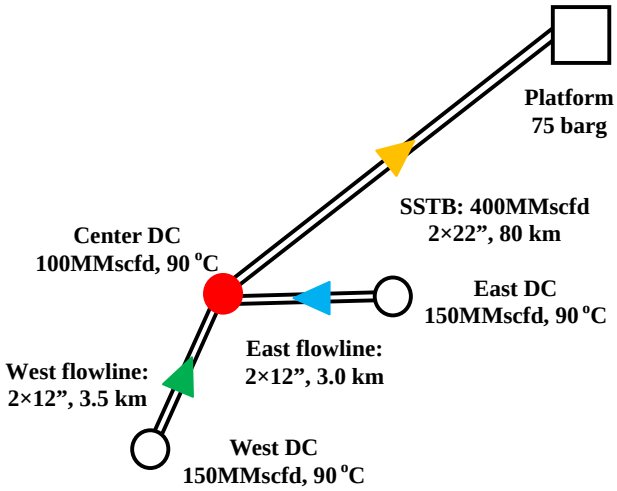

Fig. 1 Sketch map of Liwan3-1 gas field flowlines and pipelines

In this paper, a mechanistic heat transfer model of deepwater partially-buried pipeline transporting wet natural gas is developed, and the temperature profile behaviors and CRA length of Liwan3-1 gas field pipelines under different conditions are studied by numerical simulation.

* Corresponding author: wangkai@cnooc.com.cn

2 Mechanistic heat transfer model of partially-buried pipeline transporting wet natural gas

The deepwater partially-buried pipeline is sketched in Fig. 2.

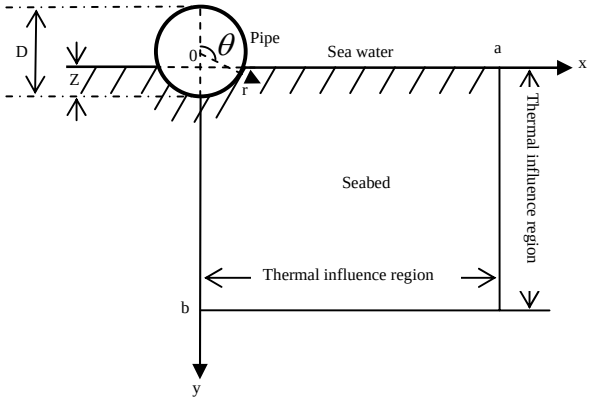

Fig. 2 Sketch map of the partially-buried pipeline

The Verley and Lund method [1] presents the following formula for calculation of static pipeline penetration:

$$\alpha = \frac{Z}{D} = 0.0071\left(S \cdot G^{0.3}\right)^{3.2} + 0.062\left(S \cdot G^{0.3}\right)^{0.7} \tag{1}$$

$$S = F_c / \left(D \cdot S_u\right) \tag{2}$$

$$G = S_u / \left(D \cdot \gamma'\right) \tag{3}$$

A comprehensive two-phase heat transfer model of the partially-buried pipeline is developed based on a mechanistic approach. The model consists of a flow pattern prediction model and a set of individual mechanistic models for predicting hydrodynamics and heat transfer. An existing mechanistic model, Gomez [2], for horizontal to vertical upward two-phase flow, is used to predict the flow pattern, liquid holdup and pressure drop.

The phase behavior model is required for determining the phase condition at any point in the pipe, the mass transfer between the phases, and the fluid properties. The phase behavior model uses the Peng and Robinson equation of state [3]. The enthalpy departure function [4] is used for the temperature change calculation.

$$\frac{\mathrm{d}h}{\mathrm{d}z} + V\frac{\mathrm{dV}}{\mathrm{d}z} + g\sin\gamma + \frac{2\pi r_i Q}{W} = 0 \tag{4}$$

$$Q = \frac{1}{\pi}\int_{-\frac{\pi}{2}}^{\frac{\pi}{2}} h_i(\theta)\left[T - T_i(\theta)\right]\mathrm{d}\theta \tag{5}$$

For the annular flow and slug flow, the Ghajar correlation [5] is used to calculate h_i, the heat transfer coefficient between the fluid with uniform temperature and the inner wall with different temperatures on circle, while the Petukhov correlation [6] is an instead for the stratified flow and dispersed bubble flow.

The heat conduction equations of the deposition layer, pipe wall and anticorrosion coating are listed below [7]:

$$\rho_j C_j \frac{\partial T_j}{\partial t} = \frac{1}{r}\frac{\partial}{\partial r}\left(\lambda_j r \frac{\partial T_j}{\partial r}\right) + \frac{1}{r^2}\frac{\partial}{\partial \theta}\left(\lambda_j \frac{\partial T_j}{\partial \theta}\right) \tag{6}$$

Where $j = 1, 2, 3$ stands for the deposition layer, pipe wall and anticorrosion coating, respectively.

The heat conduction equation of the seabed soil surrounding the pipeline is as follows [7]:

$$\rho_s C_s \frac{\partial T_s}{\partial t} = \frac{\partial}{\partial x}\left(\lambda_s \frac{\partial T_s}{\partial x}\right) + \frac{\partial}{\partial y}\left(\lambda_s \frac{\partial T_s}{\partial y}\right) \tag{7}$$

Due to symmetry of the calculation domain, only the right part is needed to be taken into consideration. The boundary conditions of the thermal-influenced region of the pipeline are written below:

$$\lambda_1 \frac{\mathrm{d}T_1}{\mathrm{d}r} = -h_i\left(T - T_i\right), \text{ at } r = r_i \tag{8}$$

$$\lambda_n \frac{\mathrm{d}T_n}{\mathrm{d}r} = -h_f\left(T_f - T_n\right) \text{ at } r = r_o \text{ and } y < 0 \tag{9}$$

$$\lambda_s \frac{\mathrm{d}T_s}{\mathrm{d}y} = h_f'\left(T_f - T_s\right), \text{ at } y = 0 \text{ and } x \geq D\sqrt{\alpha\left(1-\alpha\right)} \tag{10}$$

$$\frac{\mathrm{d}T_s}{\mathrm{d}x} = 0, \text{ at } x = 0,\ Z \leq y \leq b \text{ or } x = a \tag{11}$$

$$\frac{\mathrm{d}T_j}{\mathrm{d}\theta} = 0, \text{ at } \theta = \pm\frac{\pi}{2} \text{ and } r_i \leq r \leq r_o \tag{12}$$

$$T_s = T_c, \text{ at } y = b \tag{13}$$

Specially, only the heat conduction equations of the cross section of the pipe and seabed soil in this model are unsteady state, however, the steady results are needed. Therefore, the initial conditions of heat conduction equations can be given arbitrarily.

3 Numerical methods

A Delaunay triangulation method [8] is used to generate the grids of the seabed soil domain automatically, with which unstructured triangular grids in a Cartesian coordinate system are generated as showed in Fig. 3 (1). Since the temperature gradient is larger in the region near the pipe, denser meshes are generated in the region close to the pipeline. A structural grid generation in the polar coordinate system is applied to the steel pipe wall, deposition layer and anticorrosion coating. Fig. 3 (2) shows the annular meshes in the polar coordinate system. A finite difference method is used to discretize the pipe flow equation while a control volume method is employed to discretize the governing equations and their boundary conditions. Gauss-Seidel method is employed to solve the linear discretization equations.

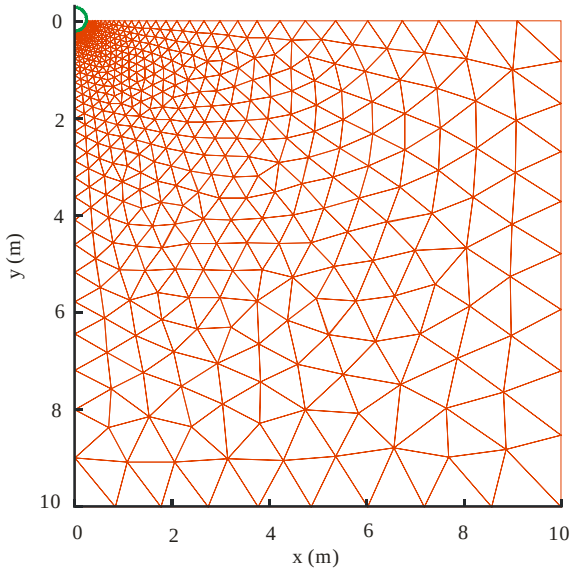

(1) Triangular grids of soil region

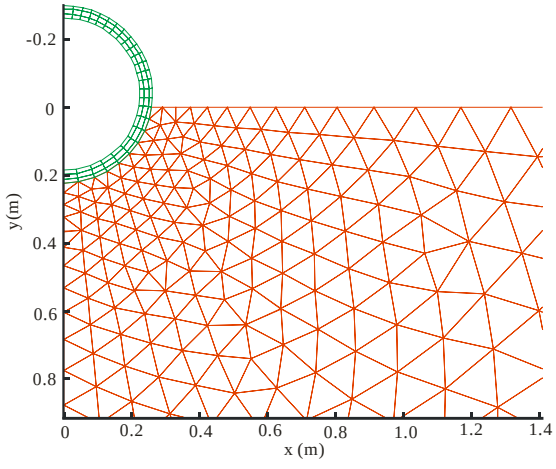

(2) Structured polar grids and the enlarged view of the unstructured grids near the pipe

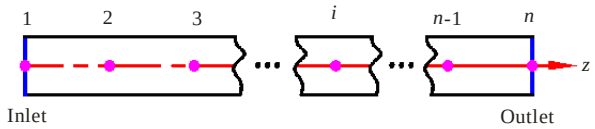

(3) Computational nodes of the pipeline

Fig. 3 Computation domain and grid generation

Uniform grids are used for spatial discretization of the pipeline as shown in Fig. 3 (3). A calculation algorithm similar to that of Mokhatab [9] was developed for the temperature profiles of partially-buried pipeline transporting wet natural gas. The biggest difference is that the calculation of the heat transfer between the pipeline and the environment. This algorithm calculates pressure and temperature along the pipeline by iteratively converging on pressure and temperature for each sequential “segment” of the pipeline. The program converges on temperature in the outer loop and pressure in the inner loop for more efficient results.

4 Analysis on CRA length of Liwan3-1 gas field pipelines

Table 1 gives the fluid compositions of Liwan3-1gas field, and Fig. 1 shows most of pipeline parameters. The subsea ambient temperature is only 3 °C. A fluctuation range of ±20% is taking account to the production rate. In addition, it is estimated conservatively that the equivalent heat conduction coefficient of seabed soil is 5 W/(m·°C), and the "critical temperature" is 23°C, which is equivalent to 20 °C temperature difference between the pipe flow and environment.

Table 1 Fluid compositions of Liwan3-1 gas field

Components	Mole %
Nitrogen	0.3348
Carbon Dioxide	3.1252
Methane	82.2025
Ethane	5.2390
Propane	1.9710
Isobutane	0.4010
Butane	0.5080
Isopentane	0.2480
Pentane	0.1870

Hexane	0.2630
Heptane	0.5060
Octane	0.5080
Nonane	0.3410
Decane	0.3210
Undecane	0.1280
Dodecane	0.1030
Tridecane	0.0710
Tetradecane	0.0470
Pentadecane	0.0510
Hexadecane	0.0280
Heptadecane	0.0140
Octadecane	0.0170
Nonadecane	0.0100
Eicosane	0.0070
C21	0.0050
C22	0.0040
C23	0.0030
C24	0.0020
C25	0.0020
C26	0.0010
C27	0.0010
Water	2.4934
MEG	0.8571
TOTAL	100

The static penetration of Liwan3-1 deepwater pipelines can be obtained directly from equation (1), in which the density and undrained shear strength of seabed soil are 1700~1900 kg/m^3 and 3~10 kPa, respectively. The production flowlines have the biggest relative buried surface area of 35%, while SSTB has the value of 39%. Thus the uniform 40% is considered in this paper.

4.1 Temperature profiles of production flowlines

Fig. 4 and Fig. 5 give the temperature profiles of east and west production flowlines, respectively. The results show that the east and west production flowlines have similar temperature profiles. The outlet temperature of east flowline is higher than that of west flowline due to slightly shorter length. For different production rates, there is significant temperature difference along the flowline, and in the outlet, the difference is enlarged to the maximum of approximately 10°C, which should be given a special attention. The higher the production rate is, the slower the temperature drop is. Therefore，the temperature drop of single flowline is relatively slower than that of double flowlines, which has an important influence on the inlet temperature and CRA length of SSTB. In most cases, the fluid temperatures of east and west production flowlines are higher than the critical temperature of 23°C, so CRA should be chosen for all production flowlines.

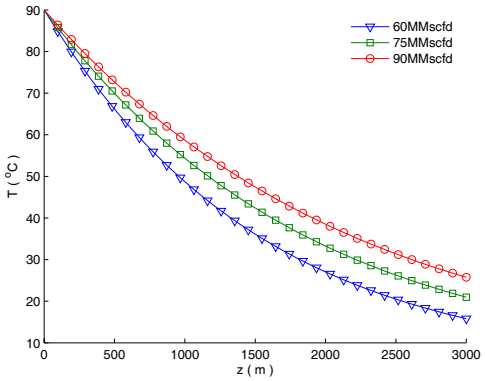

(1) Double flowlines

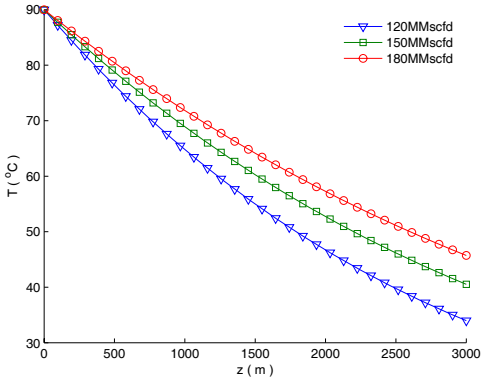

(2) Single flowline

Fig. 4 Temperature profiles of east flowline

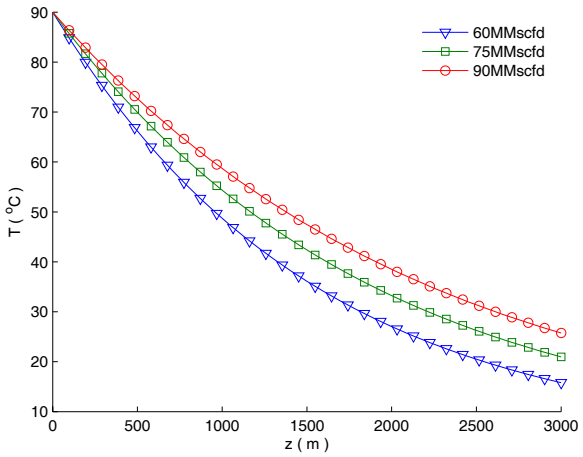

(1) Double flowline

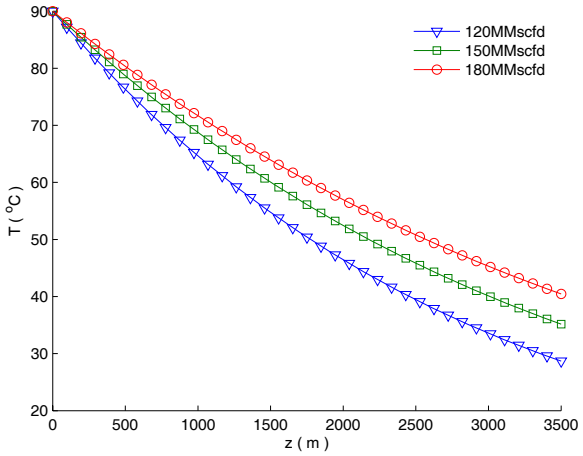

(2) Single flowline

Fig. 5 Temperature profiles of west flowline

4.2 Mixing temperature of pipeline end manifold

The production fluids of east, west and center wells will be mixing at the pipeline end manifold (PLEM) with the mass proportion of 3:3:2. Table 2 gives the mixing temperatures of PLEM at different production rates and single/double flowlines. The mixing temperatures of PLEM are equivalent to the inlet temperatures of SSTB in the following. It can be seen from Table 2 that both the production rate and single/double flowlines have a significant impact on the mixing temperatures of PLEM, with a maximum temperature difference of 22°C, and thus also on the temperature profile and CRA length of SSTB.

Table 2 Mixing temperatures of PLEM

Production rate (MMscfd)	Single/ double flowlines	Separate temperature at PLEM (°C)			Mixing temperature of PLEM (°C)
		East	West	Center	
400	Double	20.6	16.1	90	36
	Single	40.4	35.0	90	51
320	Double	15.3	11.4	90	33
	Single	33.8	28.5	90	46
480	Double	25.5	20.5	90	40
	Single	45.7	40.4	90	55

4.3 Temperature profiles of SSTB

The temperature profiles of SSTB under different production rates and single/double flowlines and pipelines are shown in Fig. 6. The results show that for the case (1), SSTB has the lowest temperature along the pipeline, thus corresponding to the shortest length of the CRA, and the temperature differences resulting from production rate almost disappear at 10 km point away from the inlet. The case (2) is similar to case (1) but has slightly higher inlet temperature due to single production flowline, resulting in a slightly longer CRA pipe. When SSTB is single pipeline, for case (3) and case (4), the temperature drops slow down, and there are remarkable temperature differences even in the 10km point. Meanwhile, the temperature along the pipeline is relatively higher and thus the CRA pipe is longer. Among all cases, case (4) has the highest temperature along pipeline and the longest CRA pipe.

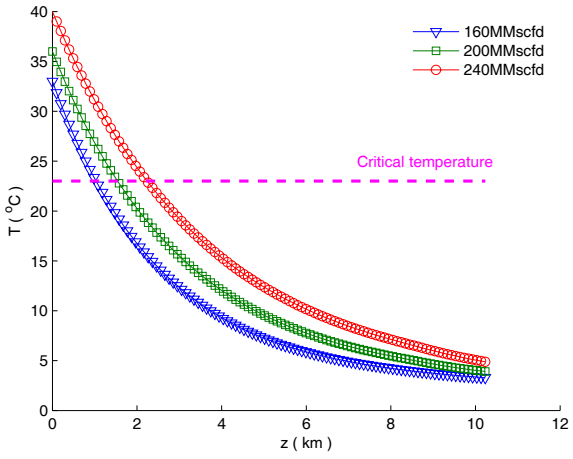

(1) Double flowlines and double pipelines

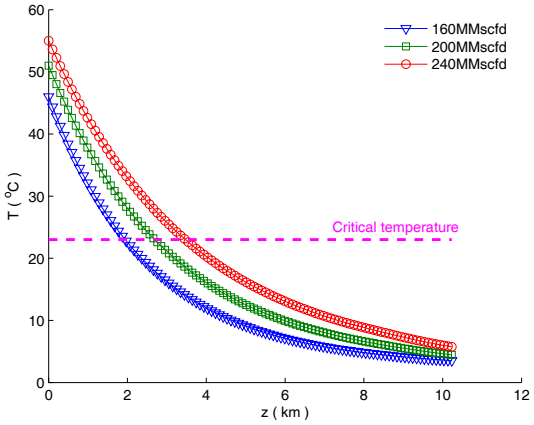

(2) Single flowline and double pipelines

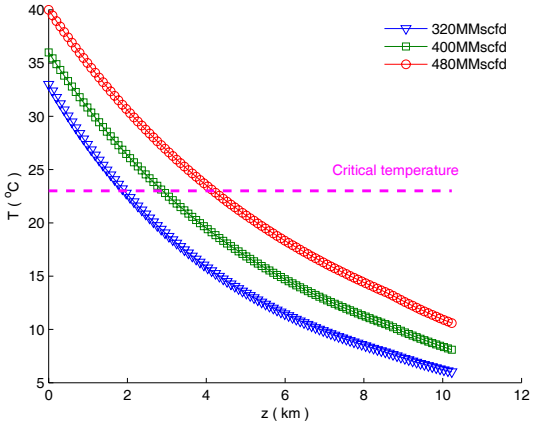

(3) Double flowlines and single pipeline

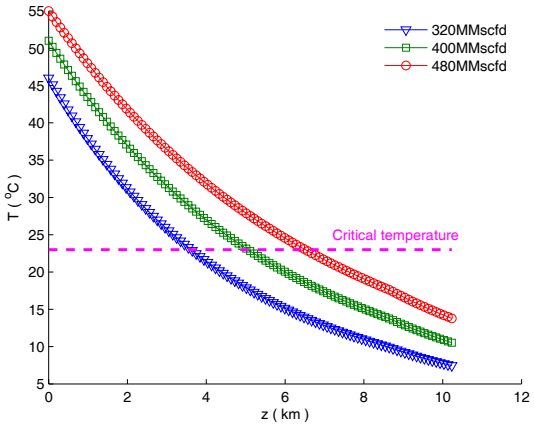

(4) Single flowline and single pipeline

Fig. 6 Temperatures profiles of SSTB

4.4 CRA length of SSTB

For a critical temperature of 23°C, from the special corrosion study of Liwan3-1 gas field project, Table 3 gives the CRA length of SSTB based on the above temperature profiles. It can be seen from Table 3 that the CRA length of high production rate and single flowline&pipeline is longer than that of low production rate and double flowlines&pipelines, and the impact of single/double flowlines or pipelines on the CRA length, in essence, can be attributed to the production rate. The maximum difference of CRA lengths is more than 5km, which gives us a great difficulty to determine the optimal CRA length but a suggestion, on the other hand, that the flow rate should be limited to a specific range for a given CRA length.

Table 3 CRA length of SSTB

Production rate (MMcfd)	Single/double SSTB	Single/double flowline	CRA length (km)
320	Double	Double	1.03
		Single	1.94
	Single	Double	1.92
		Single	3.62
400	Double	Double	1.54
		Single	2.69
	Single	Double	2.89
		Single	5.06
480	Double	Double	2.24
		Single	3.47
	Single	Double	4.18
		Single	6.51

Meanwhile, Table 4 gives the CRA length results of the PIPEFLO software with version 9.2.0 under the same condition. From Table 3 and Table 4, the CRA length of PIPEFLO is significantly shorter than that of the mechanistic heat transfer model proposed by this study. The reason is that an approximate linear heat transfer model of partially-buried pipeline is adopted by PIPEFLO, model details in ref. [10].

Table 4 CRA length of SSTB of PIPEFLO

Production rate (MMcfd)	Single/double SSTB	Single/double flowline	CRA length (km)
320	Double	Double	0.39
		Single	0.97
	Single	Double	0.83
		Single	1.85
400	Double	Double	0.68
		Single	1.36
	Single	Double	1.33
		Single	2.76
480	Double	Double	1.09
		Single	2.03
	Single	Double	2.08
		Single	3.78

5 Conclusion

(1) The accuracy of temperature profile of deepwater pipeline transporting wet natural gas has an important impact on the CRA length. A comprehensive gas-liquid two-phase heat transfer model is developed based on a mechanistic approach, which can be used to predict the temperature drop of deepwater partially-buried pipeline exactly.

(2) According to the results of mechanistic heat transfer model, a suggestion is made that for Liwan3-1gas field deepwater pipelines, all production flowlines and the upstream 1.5km of SSTB should to use CRA. Nevertheless, the production rate has to be strictly limited to no more than the design value of 400 MMscfd, and the long-term running with single flowline or pipeline is not recommended unless a low production rate comes by the end of gas field. In case the production rate is higher than 400 MMscfd, additional anticorrosion measures have to be taken.

Nomenclature

a Half width of the computational domain of the seabed soil (m)

b Depth of the computational domain of the seabed soil (m)

C_j Specific heat capacity of the j^{th} layer material, including deposition layer, pipe wall and anticorrosion coating (J/(kg·^{o}C))

C_s Specific heat capacity of the seabed soil (J/(kg·^{o}C))

D Pipeline external diameter (m)

F_c Vertical contact force (kN/m)

g Gravitational acceleration (m/s^2)

G Intermediate variable

h Specific enthalpy of the pipe flow (m^2/s^2)

h_f Heat transfer coefficient between the sea water and external wall (W/(m^2·^{o}C))

$h_{f'}$ Heat transfer coefficient between the sea water and seabed surface (W/(m^2·^{o}C))

h_i Heat transfer coefficient between the pipe flow and inner wall (W/(m^2·^{o}C))

j Natural number

Q Heat flux density between the pipe flow and inner wall (W/m^2)

r Radial direction (m)

r_i Pipeline inner radius (m)

r_o Pipeline external radius (m)

S Intermediate variable

S_u Undrained shear strength (kPa)

t Time (s)

T Average temperature of the pipe flow (^{o}C)

T_c Temperature of the constant temperature layer in the seabed soil (^{o}C)

T_f Average temperature of the sea water (^{o}C)

T_i Inner wall temperature of the pipeline (^{o}C)

T_j Temperature of the jth layer material, including deposition layer, pipe wall and anticorrosion coating (^{o}C)

T_s Seabed soil temperature (^{o}C)

V Average velocity of the pipe flow (m/s)

W Mass rate of the pipe flow (kg/s)

x Horizontal direction of the pipeline cross section (m)

y Vertical direction of the pipeline cross section (m)

z Axial direction of the pipeline (m)

Z Buried depth of the pipeline (m)

α Relative buried depth of the pipeline (m)

γ Pipeline inclination angle

γ' Submerged soil density (kN/m^3)

θ Circumferential direction of the pipeline cross section

λ_j Thermal conductivity of the jth layer material, including deposition layer, pipe wall and anticorrosion coating (W/(m·^{o}C))

λ_s Thermal conductivity of the seabed soil (W/(m·^{o}C))

π Ratio of the circumference of a circle to the diameter

ρ_j Density of the jth layer material, including deposition layer, pipe wall and anticorrosion coating (kg/m^3)

ρ_s Seabed soil density (kg/m^3)

Acknowledgments

This work is supported by the National Science & Technology Major Projects 2011ZX05026-004 and 2011ZX05056-001-01.

References

[1] Verley R. and Lund K.M. A soil resistance model for pipelines placed on clay soils. Proceedings of OMAE, Copenhagen, 1995.

[2] Gomez L.E., Shoham O. and Schmidt Z. Unified mechanistic model for steady-state two-phase flow: horizontal to vertical upward flow. SPE journal, 5(3): 339-350, 2000.

[3] Peng D.Y. and Robinson D.B. A new two-constant equation of state. Ind&eng. chem, 15: 59-64, 1976.

[4] Brill J.P. and Beggs H.D. Two-phase in pipes (6th Ed.). Tulsa, OK: Tulsa university press, 1991.

[5] Ghajar A.J. Non-boiling heat transfer in gas-liquid flow in pipes – a tutorial. J. of the Braz. Soc. of Mech. Sci. & eng., XXVII (1): 46-73, 2005.

[6] Petukhov B.S. Heat transfer and friction in turbulent pipe flow with variable physical properties. Advances in heat transfer, 6, 505-564, 1970.

[7] Wang K., Zhang J.J., Yu B., Zhou J., Qian J.H., Qiu D.P. Numerical simulation on the thermal and hydraulic behaviors of batch pipelining crude oils with different inlet temperatures. Oil & gas science and technology - Revue de l'IFP, 64, 4, 503-520, 2009.

[8] Tao W.Q. Recent Advances of numerical heat transfer. Science press, Beijing, China, 2000.

[9] Mokhatab S. Explicit method predicts temperature and pressure profliles of gas-condensate pipelines. Energy sources (part A), 29, 781-789, 2007.

[10] Bai Y. and Bai Q. Subsea engineering handbook. New York, USA: Gulf professional publishing, 2010.